RAPID COMMUNICATION

Magnetic Resonance in Medicine

Rapid pulmonary ^{129}Xe ventilation MRI of discharged COVID-19 patients with zigzag sampling

Yuan Fang[1,2] | Haidong Li[2,3] | Luyang Shen[2] | Ming Zhang[2,3] | Ming Luo[2] | Hongchuang Li[2,3] | Qiuchen Rao[2] | Qi Chen[2,3] | Yecheng Li[2,3] | Zimeng Li[1,2] | Xiuchao Zhao[2,3] | Lei Shi[2,3] | Qian Zhou[2] | Yeqing Han[2,3] | Fumin Guo[2] | Xin Zhou[2,3,4]

Correspondence
Xin Zhou, Key Laboratory of Magnetic Resonance in Biological Systems, State Key Laboratory of Magnetic Resonance and Atomic and Molecular Physics, National Center for Magnetic Resonance in Wuhan, Wuhan Institute of Physics and Mathematics, Innovation Academy for Precision Measurement Science and Technology, Chinese Academy of Sciences–Wuhan National Laboratory for Optoelectronics, Huazhong University of Science and Technology, Wuhan, 430071, China.
Email: xinzhou@wipm.ac.cn

Abstract

Purpose: To demonstrate the feasibility of zigzag sampling for 3D rapid hyperpolarized ^{129}Xe ventilation MRI in human.

Methods: Zigzag sampling in one direction was combined with gradient-recalled echo sequence (GRE-zigzag-Y) to acquire hyperpolarized ^{129}Xe ventilation images. Image quality was compared with a balanced SSFP (bSSFP) sequence with the same spatial resolution for 12 healthy volunteers (HVs). For another 8 HVs and 9 discharged coronavirus disease 2019 subjects, isotropic resolution ^{129}Xe ventilation images were acquired using zigzag sampling in two directions through GRE-zigzag-YZ. ^{129}Xe ventilation defect percent (VDP) was quantified for GRE-zigzag-YZ and bSSFP acquisitions. Relationships and agreement between these VDP measurements were evaluated using Pearson correlation coefficient (r) and Bland–Altman analysis.

Results: For 12 HVs, GRE-zigzag-Y and bSSFP required 2.2 s and 10.5 s, respectively, to acquire ^{129}Xe images with a spatial resolution of $3.96 \times 3.96 \times 10.5\,mm^3$. Structural similarity index, mean absolute error, and Dice similarity coefficient between the two sets of images and ventilated lung regions were 0.85 ± 0.03, 0.0015 ± 0.0001, and 0.91 ± 0.02, respectively. For another 8 HVs and 9 coronavirus disease 2019 subjects, ^{129}Xe images with a nominal spatial resolution of $2.5 \times 2.5 \times 2.5\,mm^3$ were acquired within 5.5 s per subject using GRE-zigzag-YZ. VDP provided by GRE-zigzag-YZ was strongly correlated ($R^2 = 0.93$, $p < 0.0001$) with that generated by bSSFP with minimal biases (bias $= -0.005\%$, 95% limit-of-agreement $= [-0.414\%, 0.424\%]$).

Conclusion: Zigzag sampling combined with GRE sequence provides a way for rapid ^{129}Xe ventilation imaging.

KEYWORDS
hyperpolarized ^{129}Xe, lung, ventilation MRI, zigzag sampling

Yuan Fang and Haidong Li contributed equally to this work.

For affiliations refer to page 9

1 | INTRODUCTION

Hyperpolarized (HP) ^{129}Xe MRI provides a way for lung ventilation imaging by directly visualizing lung regions accessed by inhaled xenon gases during a breath-hold.[1–3] Combined with thoracic ^{1}H MRI, regional lung ventilation function could be quantified as ventilation defect percentage (VDP), a physiologically relevant imaging biomarker for lung disease evaluation. During the last two decades, HP ^{129}Xe MRI has been used increasingly for assessing the pulmonary structural and functional changes in patients with asthma, chronic pulmonary obstructive diseases, idiopathic pulmonary fibrosis, cystic fibrosis, and coronavirus disease 2019 (COVID-19).[3–10] In addition, this novel technique has also been used for evaluating treatment response and/or optimizing treatment plan for various lung diseases characterized by ventilation abnormalities.[10–12] However, current ^{129}Xe ventilation imaging is still limited by long scanning times and low spatial resolution,[13–15] hindering its widespread applications.

Spatial resolution and image acquisition time are crucial for HP ^{129}Xe MR lung ventilation imaging. Currently, ^{129}Xe ventilation images were predominantly acquired with gradient-recalled echo (GRE) or balanced steady-state free precession (bSSFP) sequences under breath-hold conditions. In-plane spatial resolution of approximately 4×4 mm^2 and a slice thickness of 10–15 mm are commonly achieved during a typical data acquisition window of 8–12 s.[2,16–19] Many efforts have been devoted to enhancing the spatial resolution and reducing the image acquisition time to improve the utility and clinical uptake of HP ^{129}Xe MRI.[20–23] Recently, HP ^{129}Xe ventilation imaging with $3 \times 3 \times 3$ mm^3 nominal spatial resolution could be achieved using an ultrashort TE sequence with radial encoding[24] or spiral encoding.[15] However, these methods require long acquisition times of up to 12 s, exceeding the breath-hold capacity for most lung disease patients.

Accelerated HP ^{129}Xe MR ventilation imaging could be achieved by optimizing the k-space sampling trajectories. For example, ultra-high-speed EPI enables rapid imaging with minimal motion artifacts,[25] and spiral MRI optimizes gradient design for faster data acquisition.[14,15,26] Zigzag sampling represents another strategy for efficient k-space filling and rapid MR data acquisition.[27] The concept is similar to the readout-segmented EPI technique used in brain imaging,[28–30] although yielding different k-space trajectories. Zigzag trajectories are typically generated by swiftly oscillating the gradients during readout. This strategy has demonstrated efficacy for accelerated k-space acquisition, particularly in the case of parallel imaging.[31] For example, zigzag sampling was used for abdominal imaging with an acceleration factor of 2[27] and for brain imaging with an acceleration factor of 6.[32] Although efficient and effective, zigzag sampling has not been used for HP ^{129}Xe ventilation imaging.

Here, a sequence combining the GRE and zigzag sampling, coined GRE-zigzag, was developed and evaluated for accelerated ^{129}Xe ventilation imaging in human. By applying zigzag sampling along two encoding directions, the image acquisition time was substantially reduced, and isotropic nominal spatial resolution ^{129}Xe ventilation images were achieved. The efficacy of the proposed approach was evaluated by quantifying and comparing the image quality and the derived ventilation biomarkers with a commonly used sequence in healthy volunteers and discharged COVID-19 patients.

2 | METHODS

2.1 | Study subjects, ^{129}Xe polarization, and MRI scan

All subjects provided written informed consent to protocols approved by the institutional review board. MRI was performed on a 3T human MRI scanner (uMR 780 [Xe]; verImagin Healthcare, Wuhan, China). Isotopically enriched xenon gases (86%) were polarized using a commercial ^{129}Xe polarizer (VIP510; verImagin Healthcare). Hyperpolarized xenon gases were accumulated cryogenically and thawed into a Tedlar bag with polarization of approximately 30% for imaging. Subjects were instructed to inhale a gas mixture from a 1.0-L Tedlar bag from functional residual capacity, and MR images were acquired under breath-hold conditions. ^{129}Xe MRI was enabled using a flexible vest-shaped, two-saddle, quadratic transmit/receive coil wrapped around the chest. ^{1}H MRI was acquired in the same breath-hold of ^{129}Xe imaging using a volume coil.

Twelve healthy subjects (age $= 24.3 \pm 2.1$ years) were used to evaluate the effectiveness of the proposed zigzag sampling strategy. An 800-mL gas mixture (100 mL HP ^{129}Xe and 700 mL medical grade N$_2$) was administered to each participant for flip-angle calibration. Subsequently, each subject was instructed to inhale two doses of 800-mL gas mixtures (300 mL HP ^{129}Xe and 500 mL medical grade N$_2$) for ventilation imaging within 30 min using a conventional 3D bSSFP sequence[19] and a 3D GRE sequence with zigzag trajectories. Table 1 summarizes the image acquisition parameters for the two methods. For a fair comparison, the proposed zigzag sampling was applied in only one of the phase-encoding directions (GRE-zigzag-Y) to generate ^{129}Xe images with the same geometry parameters (i.e., FOV, matrix size, and voxel size) as 3D bSSFP.

Another 17 participants, including 8 healthy individuals (age $= 30.6 \pm 2.5$ years) and 9 discharged patients with

TABLE 1 Acquisition parameters for ^{129}Xe ventilation imaging using balanced SSFP (bSSFP), gradient-recalled echo (GRE)–zigzag-Y, and GRE-zigzag-YZ sequences.

Parameters	bSSFP	GRE-zigzag-Y	GRE-zigzag-YZ
TE (ms)	2.65	2.17	1.53
TR (ms)	5.3	4.5	3.2
Flip angle (°)	∼6	∼3	∼3
Readout duration (ms)	1.25	0.96	0.96
Dwell time (μs)	13	10	5
Matrix size	96 × 96 × 20	96 × 96 × 20	192 × 192 × 144
RealPE (Y)	96	24	48
RecPE (Y)	96	96	192
RealPE (Z)	20	20	36
RecPE (Z)	20	20	144
Effective excitations (Nex)	1920	480	1728
FOV (mm3)	380 × 380 × 210	380 × 380 × 210	480 × 480 × 360
Resolution (mm^3)	3.96 × 3.96 × 10.5	3.96 × 3.96 × 10.5	2.5 × 2.5 × 2.5
Scan duration (s)	10.2	2.2	5.5

a clinical diagnosis of COVID-19 (age = 63.2 ± 7.1 years), were scanned for ^{129}Xe ventilation imaging with isotropic spatial resolution using a 3D-GRE sequence with zigzag sampling in both phase-encoding directions (GRE-zigzag-YZ; Table 1). Gas mixtures of 300 mL HP ^{129}Xe and 500 mL medical grade N_2, and 500 mL HP ^{129}Xe and 300 mL medical grade N_2, were used for 3D bSSFP and 3D GRE-zigzag-YZ sequences, respectively, to enable sufficient SNR for ^{129}Xe images acquired at different resolution. Thoracic ^{1}H MRI was acquired using 2D-GRE (TR = 4.3 ms, TE = 2.02 ms, FOV = 380 × 380 mm^2, matrix = 96 × 96, slice thickness = 10.5 mm, flip angle = 20°, readout duration = 0.67 ms, 50% phase undersampling, and scan time of 4.4 s) and 3D-GRE (TR = 2.4 ms, TE = 0.76 ms, FOV = 480 × 480 mm^2, matrix = 192 × 192, slice thickness = 2.5 mm, flip angle = 1°, phase oversampling = 80%, readout duration = 0.67 ms, and scan time = 6.5 s) sequences, respectively. ^{129}Xe MRI with 3D bSSFP and thoracic ^{1}H-MRI with 2D-GRE sequences were sequentially acquired within the same breath-hold. Meanwhile, ^{129}Xe MRI with 3D-GRE-zigzag-YZ and thoracic ^{1}H MRI with 3D-GRE sequences were sequentially acquired in another breath-hold.

2.2 | Three-dimensional GRE sequence with zigzag sampling trajectories

Figure 1A shows the diagram of the 3D-GRE sequence with the proposed zigzag sampling trajectory. Oscillating

k-space readout trajectories were achieved by applying an additional oscillating phase-encoding gradient,[32,33] as shown in Figure 1B. The gradients for generating the zigzag trajectories can be calculated by

$$G_x = \frac{BW}{\gamma\, FOVx}, \qquad (1)$$

$$G_y(t) = \frac{BW}{\gamma\, FOVy} \sin\left(\frac{2\pi t}{T}\right), \qquad (2)$$

where T is the periodic time of the sinusoidal gradients; BW is the acquisition bandwidth; γ is the gyromagnetic ratio; and FOV_x and FOV_y denote the FOV in x and y directions, respectively. In addition, a correction factor R[27,34] was used for gradient design as follows:

$$R = RecPE/realPE, \qquad (3)$$

where RecPE represents the number of k-space lines for reconstruction; realPE denotes the number of acquired k-space lines; and R is equivalent to the acceleration factor. By considering the correction factor R, the gradient $G_y(t)$ in Eq. (2) can be rewritten as

$$G_y(t) = \frac{BW}{\gamma FOVy/R} \sin\left(\frac{2\pi t}{T}\right). \qquad (4)$$

By applying the correction factor R, the k-space trajectory is transformed to fully fill the space, which would
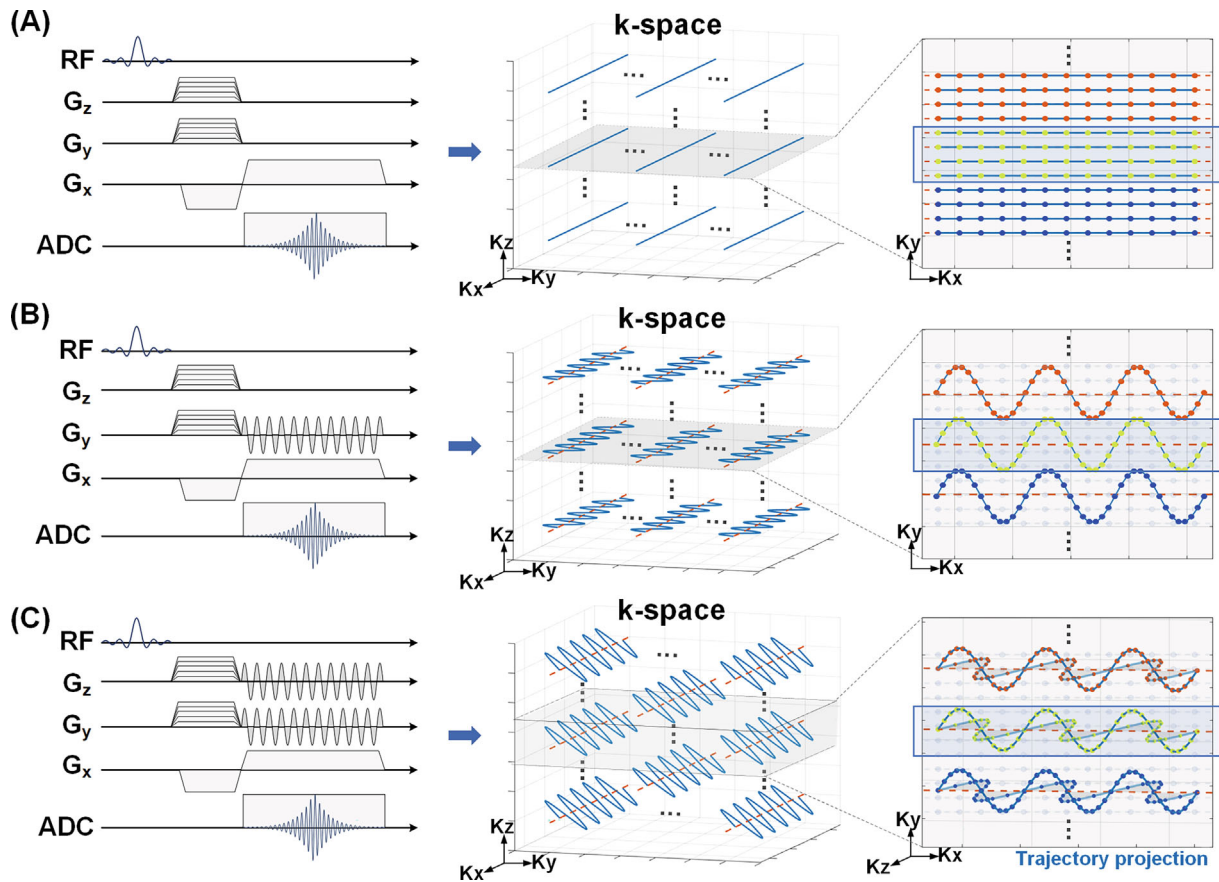
FIGURE 1 Pulse sequence diagram and k-space trajectories for conventional 3D gradient-recalled echo (GRE; A), 3D GRE-zigzag-Y ($R = 4$) (B), and 3D GRE- zigzag-YZ ($R = 4 \times 4$) (C).

reduce the aliasing artifacts in phase encoding.[32,34] In our approach, 3D zigzag k-space trajectories were implemented by applying the oscillating gradients in the two encoding directions,[33] as shown in Figure 1C. For the GRE-zigzag-Y sequence, the sinusoidal gradients for generating zigzag sampling trajectory were designed using the following parameters: the gradient amplitude (Y) was 6.38 mT/m with a slew rate of 106 mT/m/ms and the periodic time (T) is 0.24 ms. For the GRE-zigzag-YZ sequence, the amplitudes of the sinusoidal gradient for Y and Z directions were 5.05 mT/m with a slew rate of 72 mT/m/ms, and 6.74 mT/m with a slew rate of 96 mT/m/ms, respectively, and the periodic time (T) was 0.28 ms for both gradients.

2.3 | Image processing and statistical analyses

^{129}Xe and ^{1}H MR images were reconstructed offline using *MATLAB*. The data acquired with the bSSFP sequence were reconstructed using inverse fast Fourier transform. The images acquired with GRE-zigzag-Y and GRE-zigzag-YZ were regridded using nonuniform fast Fourier transform (NUFFT)[35,36] and then reconstructed using inverse fast Fourier transform. All the ^{129}Xe ventilation images were corrected for signal-intensity nonuniformity using the N4ITK bias field correction method[37] provided by the Advanced Normalization Tools (ANTS, http://stnava.github.io/ANTs/). Thoracic ^{1}H-MR images were segmented for lung cavity using a region growing method. Signal intensities in the ventilation images within the lung masks were automatically clustered into five groups corresponding to signal void (ventilation defects), hypo, middle, middle-to-high, and hyper intense signals using a k-means clustering algorithm. VDP was calculated by normalizing the volume of ventilation defects to the whole lung mask.[38,39]

For the 12 healthy volunteers, normalized SNR (SNRn) was calculated to compare the quality of the images acquired with the bSSFP and GRE-zigzag-Y sequences as follows:

$$\text{SNR}_n = \frac{\text{SNR}}{V_{\text{vox}} \times V_{\text{Xe}} \times f \times P},\tag{5}$$

where SNR was calculated using the mean of the signal intensities inside the lung divided by the SD of the noise outside the lung; V_{vox} indicates the voxel size; V_{Xe} denotes the dose of inhaled hyperpolarized xenon gas; f represents the isotopic fraction of ^{129}Xe; and P is the spin polarization.[15,24] In addition, the mean absolute error (MAE)[40] and structural similarity index measure (SSIM)[41] were used to evaluate the signal intensity and structure similarity between the images acquired with bSSFP and the GRE-zigzag-Y sequences. Rigid registration provided by ANTS was performed to align the ventilation images acquired through these methods. Moreover, ^{129}Xe ventilation images acquired through the two sequences were segmented using the 60th percentile point of signal intensities within the lung masks as previously described[42]; Dice similarity coefficient (DSC) and F1 boundary score were calculated to evaluate the spatial overlap of the two sets of ^{129}Xe image segmentation results.[43,44] SPSS (SPSS Statistics V.26.0; IBM) was used for all the statistical analyses. Paired t-tests and Wilcoxon rank-sum test were used to compare the results provided by the different methods. Linear regression and Bland–Altman analysis were used to assess the VDP measurements, and $p < 0.05$ was considered significant for all the tests.

3 | RESULTS

Figure 2 shows representative ventilation images acquired using the bSSFP and GRE-zigzag-Y sequences with the same reconstructed spatial resolution for a young healthy volunteer. For 12 healthy subjects, the SSIM, DSC, F1 boundary score, and MAE between the ventilation images acquired using the two sequences were 0.85 ± 0.03, 0.91 ± 0.01, 0.94 ± 0.02, and 0.0015 ± 0.0001, respectively. SNRn was 3.34 mL^{-2} (interquartile range: 3.09–4.86 mL^{-2}) using the bSSFP sequence and 3.26 mL^{-2} (interquartile range: 2.06–5.65 mL^{-2}) using the GRE-zigzag-Y sequence, with no significant differences between these measurements ($p = 0.875$). Similarly, VDP was $1.54 \pm 0.75\%$ when using the GRE-zigzag-Y sequence and was not significantly different ($p = 0.851$) from VDP of $1.51 \pm 0.83\%$ provided by the bSSFP method. Subtle differences between the images are probably due to partial volume effects, reconstruction algorithms, and the inevitable variations between different breath-holds.

Figure S1. shows representative ^{129}Xe ventilation images with isotropic nominal spatial resolution of $2.5 \times 2.5 \times 2.5 \text{ mm}^3$ for a healthy volunteer and a recovered COVID-19 patient. Figure 3 shows the ventilation images acquired using the bSSFP and GRE-zigzag-YZ
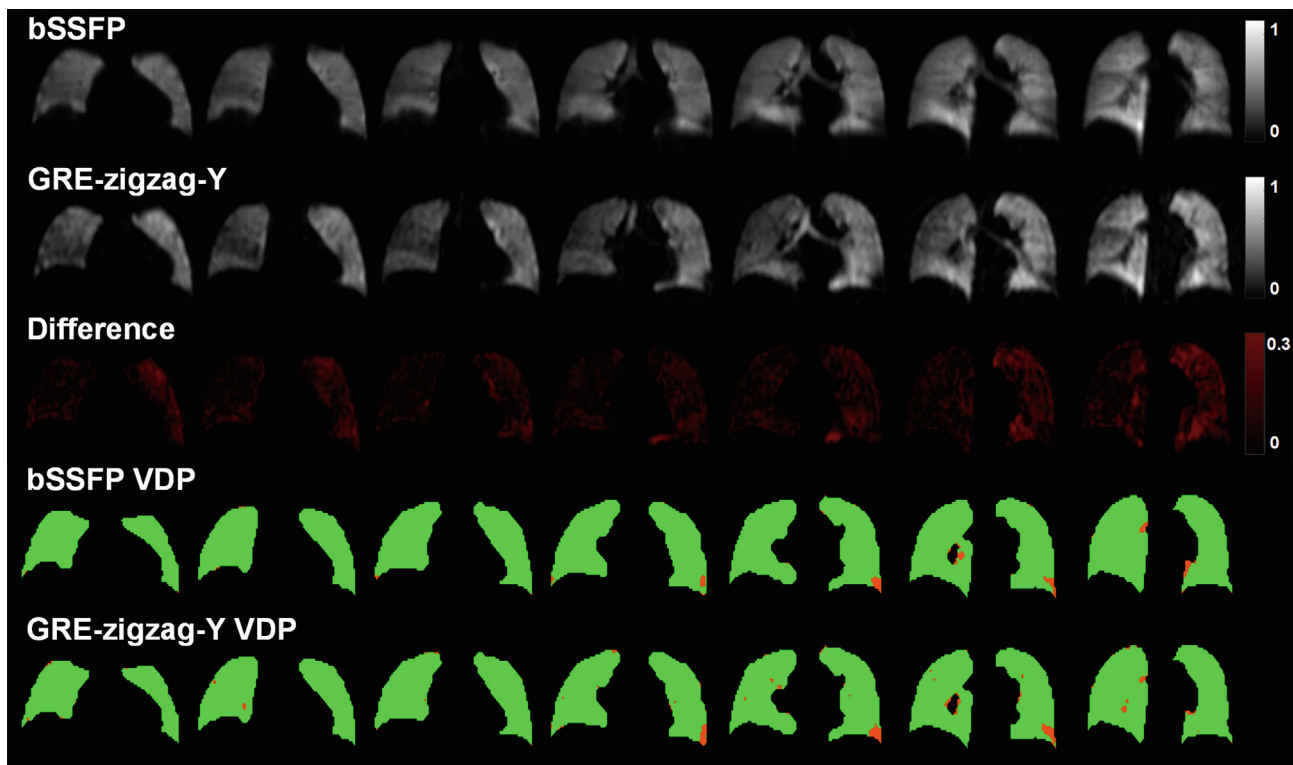

FIGURE 2 Representative ventilation images obtained with balanced SSFP (bSSFP) and the gradient-recalled echo (GRE)–zigzag-Y sequence with the same spatial resolution for a healthy subject. Differences of signal intensities and ventilation defect areas (*red*) provided by the two sequences are shown for each slice at the bottom. VDP, ventilation defect percentage.
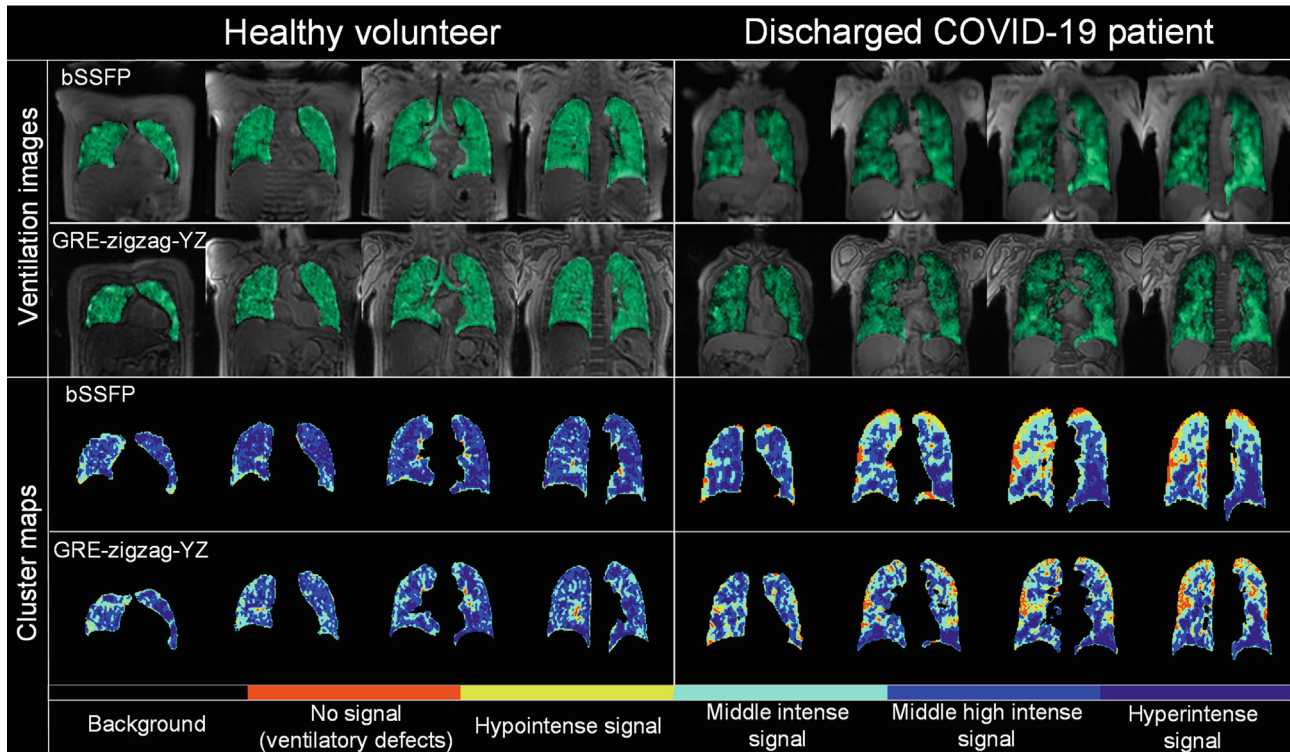
FIGURE 3 Comparison of the ventilation images and cluster maps from healthy volunteers and discharged coronavirus disease 2019 (COVID-19) patients using balanced SSFP (bSSFP) and gradient-recalled echo (GRE)–zigzag-YZ sequences. Ventilation defect, hypointense, middle intense, middle high intense, and hyperintense signal areas are marked with red, yellow, cyan, blue, and dark blue color, respectively.

sequences and the corresponding clustering maps for a healthy volunteer and a discharged COVID-19 patient. For 8 healthy volunteers and 9 discharged COVID-19 patients, SNRn was $3.13 \pm 2.14 \, \text{mL}^{-2}$ and $3.05 \pm 0.96 \, \text{mL}^{-2}$ for GRE-zigzag-YZ and bSSFP acquisitions, respectively. The measured VDP from the two groups with both methods are summarized in Table S1. Of note, these VDP measurements were not significantly different for the 8 healthy volunteers (GRE-zigzag-YZ: VDP $= 1.24 \pm 0.54\%$, bSSFP: VDP $= 1.27 \pm 0.58\%$; $p = 0.736$) and the 9 discharged COVID-19 patients (GRE-zigzag-YZ: VDP $= 7.06 \pm 2.85\%$, bSSFP: VDP $= 6.93 \pm 2.72\%$; $p = 0.444$).

VDP provided by the GRE-zigzag-YZ sequence was strongly correlated with that generated via the bSSFP acquisition ($y = 1.03x - 0.06$, $R^2 = 0.988$; $p < 0.0001$) as shown in Figure 4A. Bland–Altman analysis demonstrated a marginal bias of -0.005% (95% limits of agreement: -0.414%–0.424%) between the two sets of VDP measurements (Figure 4B).

4 | DISCUSSION

In this study, we developed a k-space sampling strategy for rapid and efficient data acquisition for isotropic nominal resolution hyperpolarized ^{129}Xe MRI in human. Our approach required 5.5 s to acquire a 3D ^{129}Xe ventilation image with an isotropic nominal spatial resolution of $2.5 \times 2.5 \times 2.5 \, \text{mm}^3$, and the image quality was similar to that provided by a commonly used bSSFP sequence. For a cohort of 8 healthy individuals and 9 discharged patients with COVID-19, the VDP measurements provided by our approach were strongly correlated with that obtained using bSSFP. These findings indicate that our approach may be suitable for rapid and isotropic nominal spatial resolution ^{129}Xe ventilation imaging while providing sufficient image quality, suggesting its potential clinical utility for lung disease patient care.

The proposed method demonstrated notable advantages in improving the nominal spatial resolution and reducing the acquisition time for ^{129}Xe MRI. Isotropic nominal spatial resolution ^{129}Xe ventilation imaging might enable us to visualize the distribution of ^{129}Xe gases in the lung with more detail, facilitating more precise quantitation of lung function.[45] As shown in Figure 5, ventilation defects could be observed in the images obtained with the GRE-zigzag-YZ sequence. However, due to partial volume effects,[15,46] ventilation defect sizes smaller than the slice thickness are hardly ever observed. In the same longitudinal observation point, areas with signals in upper layers may obscure regions without signals in lower layers, leading to the inaccurate estimate of no-signal

FIGURE 4 Comparison of the ventilation defect percentage (VDP) measured with balanced SSFP (bSSFP) and gradient-recalled echo (GRE)–zigzag-YZ sequences. Linear regression (A) and Bland–Altman analysis (B) of VDP provided by GRE-zigzag-YZ and bSSFP. COVID-19, coronavirus disease 2019.
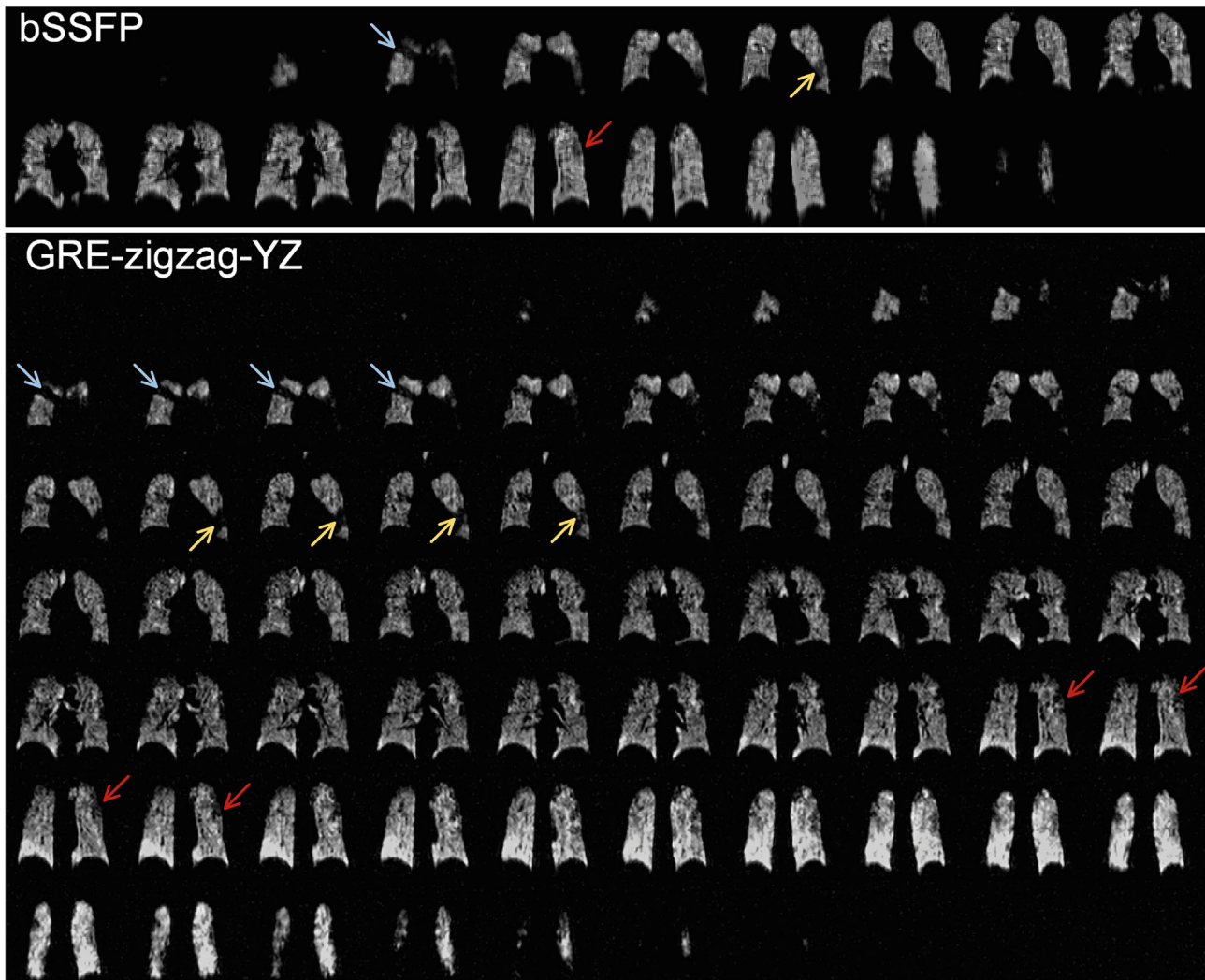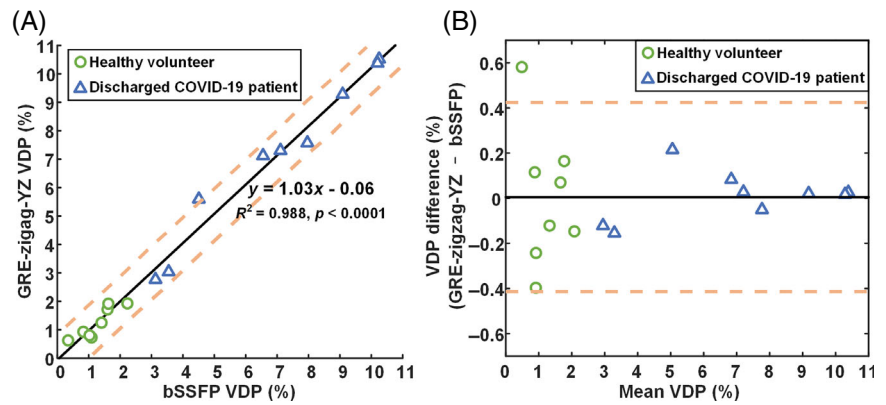

FIGURE 5 ^{129}Xe ventilation images obtained with balanced SSFP (bSSFP) and gradient-recalled echo (GRE)–zigzag-YZ for a representative coronavirus disease 2019 patient. Blue, yellow, and red arrows indicate that more details of ventilation information are observed in the images acquired with GRE-zigzag-YZ compared with bSSFP in the corresponding slices, respectively.

areas in the images obtained with the bSSFP sequence. To the best of our knowledge, this is the first demonstration of 3D ^{129}Xe ventilation imaging in human with an isotropic spatial resolution of $2.5 \times 2.5 \times 2.5$ mm^3 and

image acquisition time of 5.5 s. We note that by slightly reducing the nominal spatial resolution to $3 \times 3 \times 3$ mm^3, the acquisition time could be further shortened to 3.5 s (see Figure S2 for the imaging parameters and the

[129]Xe images). This would provide additional options for using [129]Xe MRI to assess pulmonary ventilation function and microstructure with isotropic spatial resolution in patients who have difficulties in breath-holding, such as discharged COVID-19 patients who suffer from progressive lung injuries[47–49] and reduced breath-hold capacity.[50,51]

The low MAE and high SSIM, DSC, and F1 boundary scores suggest that the quality of the [129]Xe images acquired with the GRE-zigzag-Y sequence was comparable to that obtained with the conventional bSSFP method when using the same imaging parameters (FOV, matrix sizes, and voxel sizes). However, the acquisition time using the GRE-zigzag-Y sequence was substantially shorter than that of bSSFP, suggesting greater effectiveness of zigzag versus Cartesian sampling. Compared with bSSFP, the GRE-zigzag-YZ acquisition generated [129]Xe images with similar SNRn despite a smaller RF excitation angle being used (6º for bSSFP and 3º for GRE-zigzag-YZ); this may be because of the differences in the trajectories and the image reconstruction methods.[33] The difference in HP [129]Xe doses used for bSSFP and GRE-zigzag-YZ acquisitions might introduce bias when comparing the two sets of SNRn measurements. However, it is important to note that this setting is designed primarily to ensure adequate SNR for [129]Xe images at various resolution, and the nominal voxel size for GRE-zigzag-YZ is merely about 10% of that with bSSFP. Moreover, time savings could not be obtained in bSSFP only by increasing HP [129]Xe dose. Importantly, VDP measurements provided by the GRE-zigzag-YZ sequence were strongly correlated with that generated by bSSFP, a widely used method for [129]Xe ventilation imaging in the community, with no significant differences between the sequences in 8 healthy individuals and 9 COVID-19 patients. These observations further highlight the clinical utility of the proposed zigzag sampling strategy for rapid and isotropic spatial resolution [129]Xe ventilation imaging in clinic.

The k-space data acquired in zigzag trajectories were reconstructed using NUFFT, and a large FOV was used to effectively mitigate the aliasing artifacts caused by undersampling with the zigzag trajectory. Previous studies showed that image quality could be improved by using a high degree of overgridding and an iterative density compensation function during NUFFT reconstruction.[35] In addition, use of large FOV is an effective approach for separating the regions of interest from aliasing artifacts.[52] Figure 6 show that the original reconstructed images with aliasing artifacts occurred in the peripheral areas of the FOV, but the lung was well separated from these artifacts.

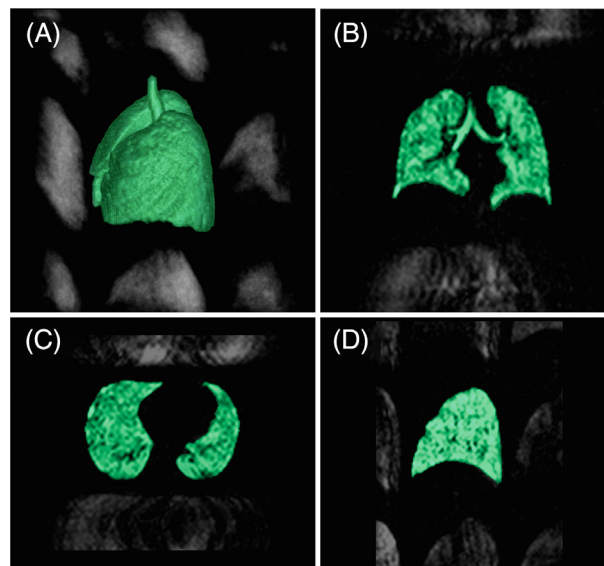This proof-of-concept study could be further expanded in several ways. The aliasing artifacts caused by

FIGURE 6 Original reconstructed [129]Xe ventilation images acquired using gradient-recalled echo–zigzag-YZ for a healthy volunteer. The lung is well separated from the surrounding aliasing artifacts as shown in 3D (A), coronal (B), transverse (C), and sagittal (D) views.

undersampling were minimized using a large FOV, which degrades the spatial resolution of the ventilation images. Undersampled reconstruction methods, including deep learning and compressed sensing, may be used for undersampled reconstruction while reducing these artifacts, enabling [129]Xe ventilation imaging with smaller FOV and higher spatial resolution. In addition, the imaging speed of [129]Xe lung MRI might be further improved by implementing parallel-imaging techniques,[27] and previous studies demonstrated that zigzag sampling can be used in parallel imaging to improve the image quality of brain ^{1}H MRI.[32] Moreover, high-performance gradients with high slew rates could be used to further improve the spatial resolution and reduce the acquisition time for [129]Xe ventilation imaging.

5 | CONCLUSION

In this study, a zigzag trajectory was used for rapid and isotropic spatial resolution [129]Xe ventilation imaging in humans. The image quality and the clinically relevant imaging biomarkers provided by this approach were highly consistent with that generated by a reference bSSFP sequence, whereas the data acquisition time was about 2 times shorter. These results suggest the clinical utility of the proposed approach for assessing lung ventilation information in patients with lung diseases, particularly in those with limited breath-holding capacity.

AFFILIATIONS

[1]School of Physics, Huazhong University of Science and Technology, Wuhan, China

[2]Key Laboratory of Magnetic Resonance in Biological Systems, State Key Laboratory of Magnetic Resonance and Atomic and Molecular Physics, National Center for Magnetic Resonance in Wuhan, Wuhan Institute of Physics and Mathematics, Innovation Academy for Precision Measurement Science and Technology, Chinese Academy of Sciences–Wuhan National Laboratory for Optoelectronics, Huazhong University of Science and Technology, Wuhan, China

[3]University of Chinese Academy of Sciences, Beijing, China

[4]School of Biomedical Engineering, Hainan University, Hainan, China

ACKNOWLEDGMENTS

ORCID

Xin Zhou https://orcid.org/0000-0002-5580-7907

REFERENCES

1. Xie J, Li H, Zhang H, et al. Single breath-hold measurement of pulmonary gas exchange and diffusion in humans with hyperpolarized Xe-129 MR. *NMR Biomed.* 2019;32:e4068.

2. He M, Driehuys B, Que LG, Huang Y-CT. Using hyperpolarized [129]Xe MRI to quantify the pulmonary ventilation distribution. *Acad Radiol.* 2016;23:1521-1531.

3. Li H, Zhao X, Wang Y, et al. Damaged lung gas exchange function of discharged COVID-19 patients detected by hyperpolarized Xe-129 MRI. *Sci Adv.* 2021;7(1):eabc8180.

4. Virgincar RS, Cleveland ZI, Sivaram Kaushik S, et al. Quantitative analysis of hyperpolarized [129]Xe ventilation imaging in healthy volunteers and subjects with chronic obstructive pulmonary disease. *NMR Biomed.* 2013;26:424-435.

5. Driehuys B, Martinez-Jimenez S, Cleveland ZI, et al. Chronic obstructive pulmonary disease: safety and tolerability of hyperpolarized Xe-129 MR imaging in healthy volunteers and patients. *Radiology.* 2012;262:279-289.

6. Walkup LL, Thomen RP, Akinyi TG, et al. Feasibility, tolerability and safety of pediatric hyperpolarized [129]Xe magnetic resonance imaging in healthy volunteers and children with cystic fibrosis. *Pediatr Radiol.* 2016;46:1651-1662.

7. Hahn AD, Carey KJ, Barton GP, et al. Hyperpolarized [129]Xe MR spectroscopy in the lung shows 1-year reduced function in idiopathic pulmonary fibrosis. *Radiology.* 2022;211433:688-696.

8. Kim M, Doganay O, Hwang HJ, Seo JB, Gleeson FV. Lobar ventilation in patients with COPD assessed with the full-scale airway network flow model and xenon-enhanced dual-energy CT. *Radiology.* 2021;298:201-209.

9. Zhang M, Li HD, Li HC, et al. Quantitative evaluation of lung injury caused by $PM_{2.5}$ using hyperpolarized gas magnetic resonance. *Magn Reson Med.* 2020;84:569-578.

10. Svenningsen S, Kirby M, Starr D, et al. Hyperpolarized [3]He and [129]Xe MRI: differences in asthma before bronchodilation. *J Magn Reson Imaging.* 2013;38:1521-1530.

11. McIntosh MJ, Kooner HK, Eddy RL, et al. Asthma control, airway mucus, and [129]Xe MRI ventilation after a single benralizumab dose. *Chest.* 2022;162:520-533.

12. Stewart NJ, Higano NS, Mukthapuram S, et al. Initial feasibility and challenges of hyperpolarized [129]Xe MRI in neonates with bronchopulmonary dysplasia. *Magn Reson Med.* 2023;90:2420-2431.

13. Li Z, Xiao S, Wang C, et al. Encoding enhanced complex CNN for accurate and highly accelerated MRI. *IEEE Trans Med Imaging.* 2024. doi:10.1109/TMI.2024.3351211

14. Zanette B, Munidasa S, Friedlander Y, Ratjen F, Santyr G. A 3D stack-of-spirals approach for rapid hyperpolarized [129]Xe ventilation mapping in pediatric cystic fibrosis lung disease. *Magn Reson Med.* 2022;89:1083-1091.

15. Willmering MM, Niedbalski PJ, Wang H, et al. Improved pulmonary [129]Xe ventilation imaging via 3D-spiral UTE MRI. *Magn Reson Med.* 2020;84:312-320.

16. Stewart NJ, Chan H-F, Hughes PJC, et al. Comparison of [3]He and [129]Xe MRI for evaluation of lung microstructure and ventilation at 1.5T. *J Magn Reson Imaging.* 2018;48:632-642.

17. Niedbalski PJ, Hall CS, Castro M, et al. Protocols for multi-site trials using hyperpolarized [129]Xe MRI for imaging of ventilation, alveolar-airspace size, and gas exchange: a position paper from the [129]Xe MRI clinical trial. *Magn Reson Med.* 2021;86:2966-2986.

18. Mugler JP, Altes TA. Hyperpolarized [129]Xe MRI of the human lung. *J Magn Reson Imaging.* 2013;37:313-331.

19. Wild JM, Teh K, Woodhouse N, et al. Steady-state free precession with hyperpolarized He-3: experiments and theory. *J Magn Reson.* 2006;183:13-24.

20. Xiao S, Deng H, Duan C, et al. Considering low-rank, sparse and gas-inflow effects constraints for accelerated pulmonary dynamic hyperpolarized Xe-129 MRI. *J Magn Reson.* 2018;290:29-37.

21. Duan C, Deng H, Xiao S, et al. Accelerate gas diffusion-weighted MRI for lung morphometry with deep learning. *Eur Radiol.* 2022;32:702-713.

22. Collier GJ, Hughes PJC, Horn FC, et al. Single breath-held acquisition of coregistered 3D [129]Xe lung ventilation and anatomical proton images of the human lung with compressed sensing. *Magn Reson Med.* 2019;82:342-347.

23. Duan C, Deng H, Xiao S, et al. Fast and accurate reconstruction of human lung gas MRI with deep learning. *Magn Reson Med.* 2019;82:2273-2285.

24. He M, Robertson SH, Kaushik SS, et al. Dose and pulse sequence considerations for hyperpolarized [129]Xe ventilation MRI. *Magn Reson Imaging.* 2015;33:877-885.

25. Butts K, Riederer SJ, Ehman RL, Thompson RM, Jack CR. Interleaved echo planar imaging on a standard MRI system. *Magn Reson Med.* 1994;31:67-72.

26. Ahn CB, Kim JH, Cho ZH. High-speed spiral-scan echo planar NMR imaging-I. *IEEE Trans Med Imaging.* 1986;5:2-7.

27. Moriguchi H, Duerk JL. Bunched phase encoding (BPE): a new fast data acquisition method in MRI. *Magn Reson Med.* 2006;55:633-648.

28. Porter DA, Heidemann RM. High resolution diffusion-weighted imaging using readout-segmented echo-planar imaging, parallel imaging and a two-dimensional navigator-based reacquisition. *Magn Reson Med.* 2009;62:468-475.

29. Holdsworth SJ, Skare S, Newbould RD, Guzmann R, Blevins NH, Bammer R. Readout-segmented EPI for rapid high resolution diffusion imaging at 3T. *Eur J Radiol.* 2008;65:36-46.

30. Yeom KW, Holdsworth SJ, Van AT, et al. Comparison of readout-segmented echo-planar imaging (EPI) and single-shot EPI in clinical application of diffusion-weighted imaging of the pediatric brain. *Am J Roentgenol.* 2013;200:W437-W443.

31. Sodickson DK, Manning WJ. Simultaneous acquisition of spatial harmonics (SMASH): fast imaging with radiofrequency coil arrays. *Magn Reson Med.* 1997;38:591-603.

32. Breuer FA, Moriguchi H, Seiberlich N, et al. Zigzag sampling for improved parallel imaging. *Magn Reson Med.* 2008;60:474-478.

33. Bilgic B, Gagoski BA, Cauley SF, et al. Wave-CAIPI for highly accelerated 3D imaging. *Magn Reson Med.* 2015;73:2152-2162.

34. In MH, Posnansky O, Speck O. High-resolution distortion-free diffusion imaging using hybrid spin-warp and echo-planar PSF-encoding approach. *Neuroimage.* 2017;148:20-30.

35. Robertson SH, Virgincar RS, He M, Freeman MS, Kaushik SS, Driehuys B. Optimizing 3D noncartesian gridding reconstruction for hyperpolarized ^{129}Xe MRI-focus on preclinical applications. *Concepts Magn Reson Part A.* 2015;44:190-202.

36. Fessler JA, Sutton BP. Nonuniform fast Fourier transforms using min-max interpolation. *IEEE Trans Signal Process.* 2003;51:560-574.

37. Tustison NJ, Avants BB, Cook PA, et al. N4ITK: improved N3 bias correction. *IEEE Trans Med Imaging.* 2010;29:1310-1320.

38. Kirby M, Heydarian M, Svenningsen S, et al. Hyperpolarized He-3 magnetic resonance functional imaging semiautomated segmentation. *Acad Radiol.* 2012;19:141-152.

39. Zha W, Niles DJ, Kruger SJ, et al. Semiautomated ventilation defect quantification in exercise-induced bronchoconstriction using hyperpolarized helium-3 magnetic resonance imaging: a repeatability study. *Acad Radiol.* 2016;23:1104-1114.

40. Zhang H, Xie J, Xiao S, et al. Lung morphometry using hyperpolarized Xe-129 multi-b diffusion MRI with compressed sensing in healthy subjects and patients with COPD. *Med Phys.* 2018;45:3097-3108.

41. Wang Z, Bovik AC, Sheikh HR, Simoncelli EP. Image quality assessment: from error visibility to structural similarity. *IEEE Trans Image Process.* 2004;13:600-612.

42. Thomen RP, Walkup LL, Roach DJ, Cleveland ZI, Clancy JP, Woods JC. Hyperpolarized Xe-129 for investigation of mild cystic fibrosis lung disease in pediatric patients. *J Cystic Fibrosis.* 2017;16:275-282.

43. Dice LR. Measures of the amount of ecologic association between species. *Ecology.* 1945;26:297-302.

44. Csurka G, Larlus D, Perronnin F. What is a good evaluation measure for semantic segmentation? In: 24th British Machine Vision Conference, Bristol, England, 2013. Corpus ID: 10670873.

45. Zha W, Kruger SJ, Cadman RV, et al. Regional heterogeneity of lobar ventilation in asthma using hyperpolarized Helium-3 MRI. *Acad Radiol.* 2018;25:169-178.

46. González Ballester MÁ, Zisserman AP, Brady M. Estimation of the partial volume effect in MRI. *Med Image Anal.* 2002;6:389-405.

47. Luger AK, Sonnweber T, Gruber L, et al. Chest CT of lung injury 1 year after COVID-19 pneumonia: The CovILD study. *Radiology.* 2022;304:462-470.

48. McDonald LT. Healing after COVID-19: are survivors at risk for pulmonary fibrosis? *Am J Physiol Lung Cell Molec Physiol.* 2021;320:L257-L265.

49. Guziejko K, Moniuszko-Malinowska A, Czupryna P, et al. Assessment of pulmonary function tests in COVID-19 convalescents six months after infection. *J Clin Med.* 2022;11:7052.

50. Marks B, Mitchell DG, Simelaro JP. Breath-holding in healthy and pulmonary-compromised populations: effects of hyperventilation and oxygen inspiration. *J Magn Reson Imaging.* 1997;7:595-597.

51. Gong G, Yin Y. SU-E-T-326: the oxygen saturation (SO2) and breath-holding time variation applied active breathing control (ABC). *Med Phys.* 2014;41:299.

52. Goldfarb JW. The SENSE ghost: field-of-view restrictions for SENSE imaging. *J Magn Reson Imaging.* 2004;20:1046-1051.

SUPPORTING INFORMATION

Additional supporting information may be found in the online version of the article at the publisher's website.

Figure S1. Typical high-spatial-resolution ventilation images acquired from a healthy volunteer and a discharged patient with coronavirus disease 2019 (COVID-19). The isotropic images were acquired from a healthy volunteer (29 year-old male) and a discharged COVID-19 patient (68 year-old female) within 5.5 s, and the spatial resolution was $2.5 \times 2.5 \times 2.5$ mm^3. The measured SNRs were 2.28 and 1.57 mL^{-2}, and the measured ventilation defect percentages (VDP) were 0.73% and 7.12%, for the healthy volunteer and the discharged COVID-19 patient, respectively.

Figure S2. Typical ventilation images acquired from a healthy volunteer with an isotropic spatial resolution of $3 \times 3 \times 3$ mm^3 and acquisition time of 3.5 s. Sequence acquisition: TR $= 2.9$ ms, TE $= 1.4$ ms, matrix $= 160 \times 160 \times 120$, effective excitations $= 1200$, resolution $= 3 \times 3 \times 3$ mm^3, flip angle $= \sim 3°$, dwell time $= 5$ μs, and scan time $= 3.5$ s.

Figure S3. The transverse (A) and longitudinal (B) cross-sectional line profiles of ventilation images using balanced SSFP (bSSFP) and gradient-recalled echo (GRE)–zigzag-Y sequences.

Table S1. Demographics, pulmonary function tests (PFTs), and ventilation analysis results for healthy volunteers and discharged patients with coronavirus disease 2019 (COVID-19).